Available online at www.sciencedirect.com
SCIENCE DIRECT®
Journal of Solid State Chemistry 173 (2003) 367–373
JOURNAL OF SOLID STATE CHEMISTRY
http://elsevier.com/locate/jssc

Synthesis, structure and magnetic characterization of a one-dimensional iron phosphate, $[NH_3CH_2CH_2CH(NH_3)CH_2CH_3]^{2+}\,{}^1_\infty[FeF(HPO_4)_2]^{2-}$

Sukhendu Mandal,[a] Srinivasan Natarajan,[a,b,*] Wilhelm Klein,[b] Martin Panthöfer,[b] and Martin Jansen[b,1]

[a] *Chemistry and Physics of Materials Unit, Framework Solids Laboratory, Jawaharlal Nehru Centre for Advanced Scientific Research, Jakkur P.O., Bangalore 560 064, India*
[b] *Max-Planck-Institut für Festkörperforschung, Heisenbergstrasse 1, D-70569 Stuttgart, Germany*

Received 12 September 2002; received in revised form 13 February 2003; accepted 20 February 2003

Abstract

The hydrothermal synthesis, structure and magnetic studies of a one-dimensional iron fluro-phosphate, $[NH_3CH_2CH_2CH(NH_3)CH_2CH_3]^{2+}\,{}^1_\infty[FeF(HPO_4)_2]^{2-}$, **I**, is presented. The structure, solved by single-crystal X-ray diffraction, consists of isolated ${}^1_\infty[FeF(HPO_4)_2]^{2-}$ chains of the tancoite type with diprotonated amine molecules situated in between. Magnetic studies indicate anti-ferromagnetic interactions. Crystal data: space group = $P2_1/m$ (no. 12), $a = 8.846(2)$ Å, $b = 7.211(1)$ Å, $c = 9.893(2)$ Å, $\beta = 97.10(3)^\circ$, $V = 626.2(2)$ Å^3, $Z = 4$, $\rho_{calc} = 1.968$ g cm^{-3}, $\mu(MoK\alpha) = 1.511$ mm^{-1}, $R_1 = 0.044$, $wR_2 = 0.099$, $S = 1.016$ for 134 parameters.

1. Introduction

Naturally occurring iron phosphate minerals exhibit wide compositional variety and structural diversity [1]. Synthetic iron phosphates, on the other hand, are being investigated only recently. The hydrothermal syntheses of iron phosphates have, so far, given rise to new solids possessing one- [2–5], two- [5–15] and three-dimensional [16–29] structures. The variable oxidation state coupled with the coordination preferences of iron, the broad structural variability, is one of the reasons for the continuing interest. Additionally, the structural chemistry of iron phosphates is likely to be more interesting, compared to aluminosilicate or aluminophosphate chemistry. Recently, we have begun an exploratory hydrothermal study of the synthesis of iron phosphates employing coordination complexes of iron as a starting material. During hydrothermal treatment the metal complexes, probably, release the metal ions slowly into the solution thereby facilitating the formation of unusual structures. Our initial studies resulted in the isolation new iron phosphates with one- [5], two- [5,6] and three-dimensional [17,18] structures. In continuation of this theme, we have been investigating the formation of iron phosphates using iron acetylacetonate [Fe(acac)$_3$] as the starting source of iron in the presence of 1,3-diaminopentane employing hydrothermal methods. Our efforts have yielded a new one-dimensional iron phosphate, $[NH_3CH_2CH_2CH(NH_3)CH_2CH_3]^{2+}\,{}^1_\infty[FeF(HPO_4)_2]^{2-}$, **I**, with a tancoite related structure [30]. Synthesis, structure and magnetic properties of this compound are presented in this paper.

2. Experimental

The title compound was synthesized under hydrothermal conditions starting from a coordination complex of Fe^{3+}, [Fe(acac)$_3$] as the source of iron. In a typical synthesis, 0.395 g of Fe(acac)$_3$ were dispersed in 4 mL of deionized water. 0.32 mL of H_3PO_4 (85%) and

*Corresponding author. Chemistry and Physics of Materials Unit, Framework Solids Laboratory, Jawaharlal Nehru Centre for Advanced Scientific Research, Jakkur P.O., Bangalore 560 064, India. Fax: +91-80-8642766.
E-mail addresses: raj@jncasr.ac.in (S. Natarajan), m.jansen@fkf.mpg.de (M. Jansen).
[1] Also for correspondence.

0022-4596/03/$ - see front matter © 2003 Elsevier Science (USA). All rights reserved.
doi:10.1016/S0022-4596(03)00113-0

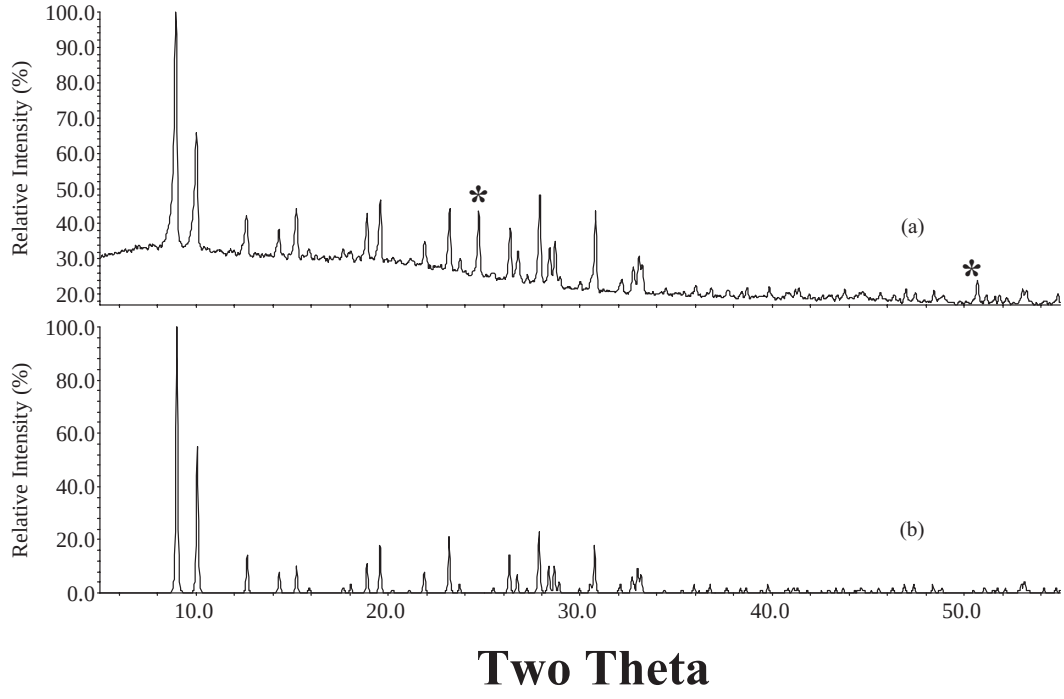

Fig. 1. Powder X-ray diffraction (Cu$K\alpha$, $\lambda = 1.540598$ Å) pattern of **I**, $[NH_3CH_2CH_2CH(NH_3)CH_2CH_3]^{2+}\ {}^{1}_{\infty}[FeF(HPO_4)_2]^{2-}$ (a) experimental (b) simulated. *Indicates as yet unidentified second phase.

0.15 mL of HF (48%) were added under continuous stirring. Finally, 0.27 mL of 1,3-diaminopentane was added to the above and the mixture was homogenized for 20 min at room temperature. All the chemicals were obtained from Aldrich, USA and were used without further purifications. The final orange colored liquid of composition $Fe(acac)_3$:$4.5H_3PO_4$:2(1,3-diaminopentane):$4HF$:$200H_2O$ was transferred in to a 23 mL PTFE-lined stainless steel autoclave (Parr, Moline, USA) and heated at 150°C for 96 h. The resulting product, consisting of large quantities of very small, micro-crystalline needle like colorless single crystals, was vacuum filtered, washed with plenty of deionized water and dried at ambient conditions. The initial and final pH of the reaction mixture was found to be around 2, therefore no appreciable change in the pH occurred.

The iron phosphate, $[NH_3CH_2CH_2CH(NH_3)CH_2CH_3]^{2+}\ {}^{1}_{\infty}[FeF(HPO_4)_2]^{2-}$, **I**, was characterized using a variety of analytical methods. An EDAX analysis indicated a Fe:P ratio of 1:2, and in addition indicated the presence of fluorine. A chemical analysis also confirmed the presence of fluorine (obs. 5.2%, calc. 5.6%) [14]. Elemental analysis, found: C16.29, N7.7, H4.95%; calcd: C16.17, N7.55, H4.85%. IR bands: $\nu(NH) = 1550\ cm^{-1}$, $\nu(CN) = 1179\ cm^{-1}$, $\nu(CH) = 1470\ cm^{-1}$, $\nu(P–OH) = 1626\ cm^{-1}$. **I** was further characterized by means of powder X-ray diffraction (XRD, STOE-Stadi P diffractometer, germanium monochromator, Cu$K\alpha$ radiation, $\lambda = 1.540598$ Å, linear position sensitive detector, Si as an external standard), thermogravimetric analysis (TGA, Mettler-Toledo, TG850) and magnetic investigations using a Squid magnetometer (Quantum Design MPMS; 5–360 K). The powder XRD pattern exclusively exhibited reflection of a hitherto unknown material; the pattern was entirely consistent with the structure determined by means of single-crystal X-ray diffraction. A typical powder X-ray data for **I** is presented in Fig. 1.

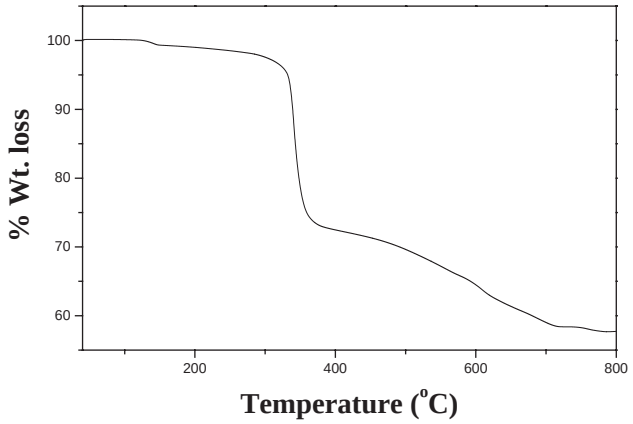

Fig. 2. The TGA curve for **I**, $[NH_3CH_2CH_2CH(NH_3)CH_2CH_3]^{2+}\ {}^{1}_{\infty}[FeF(HPO_4)_2]^{2-}$.

TGA was carried out in O_2 atmosphere (flow rate = 50 mL/min) in the range 30–800°C (heating rate = 5°C/min). The thermal analysis exhibited one sharp weight loss followed by a continuous decrease (Fig. 2). The weight loss of 27.1% in the region

325–350°C is in good agreement with the loss of one equivalent of 1,3-diaminopentane (calcd. 28%). The tail, occurring in the region between 400°C and 700°C (obsd. 14.1%), corresponds to the condensation of the hydrogen phosphate along with the loss of the fluorine (calc. 14.2%). It is likely that the water molecules formed during the combustion of the organic molecules hydrolyzes the fluoride in the framework, resulting in the formation of volatile hydrogen fluoride. The calcined sample is amorphous to powder XRD.

3. Single-crystal structure determination

A suitable single crystal ($0.02 \times 0.02 \times 0.02\,mm^3$) was carefully isolated under a polarizing microscope and intensities were collected on a STOE IPDS-2 two-circle diffraction system for $4.09 \leqslant 2\theta^\circ \leqslant 54.7$ ($d = 100$ mm) in the ω-scan mode ($0 \leqslant \omega/^\circ \leqslant 150$, $\Delta\omega = 1^\circ$) for two different orientations ($\phi = 0^\circ, 90^\circ$) using Mo$K\alpha$ radiation ($\lambda = 0.71073$ Å). Due to the extremely small size of the crystal, the exposure time was $t = 20$ min for each frame. A numerical absorption correction was applied using an optimized crystal description (20 faces, 32 corners, 50 edges) [31] (Table 1)

Table 1
Crystal data and structure refinement parameters for **I**, $[NH_3CH_2CH_2CH(NH_3)CH_2CH_3]^{2+}\,{}^1_\infty[FeF(HPO_4)_2]^{2-}$

Empirical formula	$C_5H_{18}F_1Fe_1N_2O_8P_2$
Crystal system	Monoclinic
Space group	$P2_1/m$ (no. 12)
Crystal size (mm)	$0.02 \times 0.02 \times 0.02$
a (Å)	8.846(3)
b (Å)	7.211(1)
c (Å)	9.893(2)
β (deg)	97.10(3)
Volume (Å^3)	626.2(2)
Z	4
Formula mass	371.1
ρ_{calc} (g cm^{-3})	2.368
λ (Mo$K\alpha$) Å	0.71073
μ (mm^{-1})	3.848
2θ range (deg)	4–55
Total data collected	8667
Index ranges	$-11 \leqslant h \leqslant 11$, $-8 \leqslant h \leqslant 9$, $-12 \leqslant l \leqslant 12$
Unique data	1546
Refinement method	Full-matrix least-squares on $\|F\|^2$
R_{merg}	0.0798
R indexes [$I > 2\sigma(I)$]	$R_1 = 0.044$[a], w$R_2 = 0.099$[b]
R (all data)	$R_1 = 0.066$, w$R_2 = 0.11$
Goodness of fit (S_{obs})	1.016
No. of variables	134
Largest difference map	
Peak and hole e Å^{-3}	0.605 and –0.552 eÅ^{-3}

[a] $R_1 = \sum||F_o| - |F_c||/\sum|F_o|$;
[b] $wR_2 = \sum[w(F_o^2 - F_c^2)^2]/\sum[w(F_o^2)^2]^{1/2}$, $w = 1/[\sigma^2(F_o)^2 + (aP)^2 + bP]$, $P = [\max.(F_o^2, 0) + 2(F_c)^2]/3$, where $a = 0.0651$ and $b = 0.0$ for **I**.

Table 2
Atomic coordinates ($\times 10^4$) and equivalent isotropic displacement parameters (Å$^2 \times 10^3$) for **I**, $[NH_3CH_2CH_2CH(NH_3)CH_2CH_3]^{2+}\,{}^1_\infty[FeF(HPO_4)_2]^{2-}$

Atom	x	y	z	U_{eq}[a]
Fe(1)	5000	0	10000	16(1)
P(1)	2109(1)	2500	8546(1)	18(1)
P(2)	6122(1)	2500	7528(1)	18(1)
F(1)	5351(3)	2500	10,799(3)	21(1)
O(2)	5947(3)	762(4)	8374(3)	28(1)
O(3)	2929(3)	765(4)	9137(3)	24(1)
O(4)	456(4)	2500	8743(4)	26(1)
O(5)	2174(5)	2500	6952(4)	29(1)
O(6)	5040(5)	2500	6241(4)	33(1)
O(7)	7767(5)	2500	7077(4)	27(1)
N(1)	4190(5)	2500	3474(5)	25(1)
C(1)	2560(6)	2500	3660(6)	30(1)
C(2)	1558(7)	2500	2308(6)	27(1)
C(3)	−65(8)	2500	2454(7)	75(4)
N(2)	−1034(6)	2500	1098(5)	24(1)
C(4)	−693(9)	1884(12)	3617(8)	32(2)
C(5)	−2359(8)	2500	3709(7)	49(2)

[a] U_{eq} is defined as one third of the trace of the orthogonalized U_{ij} tensor.

The structure was solved and refined using the SHELXTL-PLUS suite of programs [32]. The systematic absences in the reduced data ($0k0$, $k = 2n+1$) indicated space groups $P2_1$ or $P2_1/m$. The structure could be solved in both the space groups. The direct methods solution readily revealed sufficient fragments of the structure (Fe, P and O) and enabled the remainder of the non-hydrogen atoms to be located from difference Fourier maps. In the case of $P2_1$ the refinement resulted in large thermal parameters, higher final R values and coupling between some sites. In $P2_1/m$, we find that one of the carbon atoms of the amine molecule [C(4)] was disordered. Most of the hydrogen positions were found from the difference Fourier map. Fluorine positions in **I** were attributed by considering the results of the chemical analysis, the bond–valence sum calculations [33] and the thermal parameter values. Final refinements included atomic positions for all the atoms and anisotropic thermal parameters for all non-hydrogen atoms and isotropic thermal parameters for all the hydrogen atoms. The final atomic coordinates and selected bond distances for **I** are presented in Tables 2 and 3.

4. Results and discussion

The asymmetric unit of **I** contains 17 non-hydrogen atoms, of which 10 atoms belong to the framework and 7 atoms to the guest species. There are one crystallographically independent Fe and two P atoms. The iron atom is coordinated with 4 oxygen and 2 fluorine atoms

Table 3
Selected bond distances (Å) and angles (deg) for **I**, $[NH_3CH_2CH_2CH(NH_3)CH_2CH_3]^{2+}\,{}^{1}_{\infty}[FeF(HPO_4)_2]^{2-}$

Bond	Distance	Bond	Distance
Fe(1)–O(2)	1.981(3) [0.5578]	P(1)–O(3)#2	1.526(3) [1.235]
Fe(1)–O(2)#1	1.981(3) [0.5578]	P(1)–O(3)	1.526(3) [1.235]
Fe(1)–O(3)#1	2.000(3) [0.5299]	P(1)–O(5)	1.585(4) [1.053]
Fe(1)–F(1)	1.977(4) [0.4469]	**Σ(P–O)**	**[4.850]**
Fe(1)–F(1)#1	1.977(4) [0.4469]	P(2)–O(6)	1.495(4) [1.343]
Fe(1)–O(3)	2.000(3) [0.5299]	P(2)–O(2)	1.525(3) [1.238]
Σ(Fe–O/F)	**[3.072]**	P(2)–O(2)#2	1.525(3) [1.238]
P(1)–O(4)	1.499(4) [1.327]	P(2)–O(7)	1.574(4) [1.085]
		Σ(P–O)	**[4.904]**
Angle	Amplitude (deg)	Angle	Amplitude (deg)
O(2)–Fe(1)–F(1)#1	89.4(1)	O(4)–P(1)–O(3)#2	112.1(2)
O(2)#1–Fe(1)–F(1)	89.4(1)	O(4)–P(1)–O(3)	112.1(2)
F(1)#1–Fe(1)–O(4)	88.9(3)	O(3)#2–P(1)–O(3)	110.1(2)
O(2)#1–Fe(1)–F(1)#1	90.6(1)	O(4)–P(1)–O(5)	106.6(2)
F(1)#1–Fe(1)–F(1)	180.0	O(3)#2–P(1)–O(5)	107.9(2)
O(2)–Fe(1)–F(1)	90.6(1)	O(3)–P(1)–O(5)	107.9(2)
O(2)–Fe(1)–O(2)#1	180.0	O(6)–P(2)–O(2)	111.7(2)
F(1)#1–Fe(1)–O(3)#1	90.6(1)	O(6)–P(2)–O(2)#2	111.7(2)
O(2)–Fe(1)–O(3)#1	88.06(2)	O(2)–P(2)–O(2)#2	110.5(2)
O(2)#1–Fe(1)–O(3)#1	91.9(4)	O(6)–P(2)–O(7)	106.0(2)
F(1)#1–Fe(1)–O(3)	89.45(1)	O(2)–P(2)–O(7)	108.4(2)
F(1)–Fe(1)–O(3)	90.6(2)	O(2)#2–P(2)–O(7)	108.4(2)
O(2)–Fe(1)–O(3)	91.9(4)	Fe(1)–O(2)–P(2)	139.1(2)
O(2)#1–Fe(1)–O(3)	88.06(2)	Fe(1)–O(3)–P(1)	139.2(2)
O(3)#1–Fe(1)–O(3)	180.0	Fe(1)#3–F(1)–Fe(1)	131.5(2)

Values in brackets are the bond valences. Their sum SVB appears in bold type at the end of the list of the distances around every cations.
#1 $-x+1, -y, -z+2$; #2 $x, -y+1-2, z$; #3 $-x+1, y+1/2, -z+2$.

forming an octahedron with average Fe–O/F distances of 1.986 Å. The O/F–Fe–O/F bond angles are in the range 88.06(2)–180°. The iron atom makes four Fe–O–P linkages to two distinct P atom neighbors with an average Fe–O–P bond angle of 139.1° and two Fe–F–Fe linkages. The iron atoms are linked together through the fluorine atoms forming infinite Fe–F–Fe one-dimensional chains. Each phosphorous atom makes two P–O–Fe bond and possesses two terminal P–O linkages. The average P–O distances and O–P–O bond angles are 1.534 Å and 109.4°, respectively. The terminal P(1)–O(5) and P(2)–O(7) bonds with distances of 1.585(4) and 1.574(4) Å are P–OH linkages. One hydrogen position near each of the oxygen atoms O(5) and O(7) was located from difference Fourier maps. The remaining terminal bonds, P(1)–O(4) and P(2)–O(6), with distances of 1.499(4) and 1.495(4) Å, are P=O linkages. Similar P–O bond distances and bond angles have been observed in many of he iron phosphate based open-framework materials [2–30]. Bond valence sum calculations [33] are in good agreement with the above and clearly indicate the oxidation state of +3 for the Fe ion. The complete list of bond distances along with their bond valence sum (SBV) values are given in Table 3.

The structure of $[NH_3CH_2CH_2CH(NH_3)CH_2CH_3]^{2+}\,{}^{1}_{\infty}[FeF(HPO_4)_2]^{2-}$, **I**, is built up from isolated infinite $[FeF(HPO_4)_2]^{2-}_{\infty}$ chains in the *ab* plane (Fig. 3). Each ${}^{1}_{\infty}[FeF(HPO_4)_2]^{2-}$ chain is built up from a central core constituted by a continuous string of FeO_4F_2 octahedra linked through their fluorine apices. The HPO_4 tetrahedra are grafted such that each iron octahedron shares its four oxygen atoms with four distinct phosphorous tetrahedra. Two consecutive octahedra are linked by two distinct tetrahedra as shown in Fig. 3. The ${}^{1}_{\infty}[FeF(HPO_4)_2]^{2-}$ are separated by the amine molecules situated in between the chains (Fig. 4). The projection of the structure down the chain axis along the *ac* plane is shown in Fig. 5.

The formation of octahedral files of the type in **I** has been observed in many of the ULM type compounds [34,35] and in some minerals [30]. In minerals, usually, hydroxyl group substitutes for the fluorine atom. The iron phosphate structure **I** is similar to the aluminum phosphate mineral tancoite, $[LiNa_2HAl(PO_4)_2OH]$, discovered at the Tanco Mines, Bernic Lake, Manitoba [36]. Similar chains have also been encountered in other phosphates, sulfate and silicate minerals [30]. These one-dimensional compounds generally exhibit the composition, $[M(TO_4)_2L]_n$ (M and T are cations of different coordination, usually octahedral and tetrahedral, L = anionic ligand, e.g., O^{2-}, OH^- or F^-). Iron phosphates with tancoite structure prepared in the

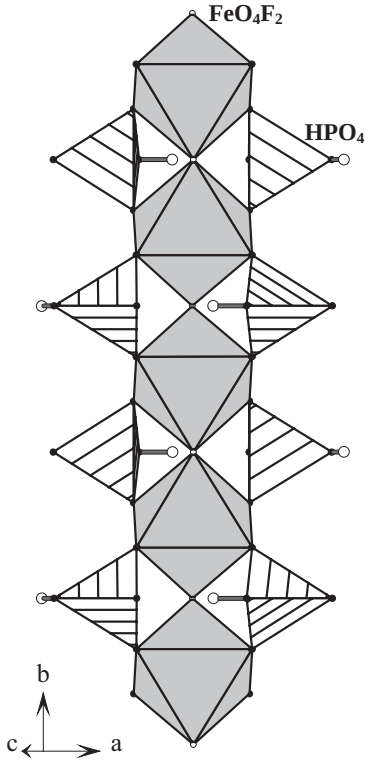

Fig. 3. Polyhedral connectivity of **I**, $[NH_3CH_2CH_2CH(NH_3)CH_2CH_3]^{2+}\,{}^{1}_{\infty}[FeF(HPO_4)_2]^{2-}$, in the *ab* plane showing the one-dimensional ${}^{1}_{\infty}[FeF(HPO_4)_2]^{2-}_{n}$ chain units.

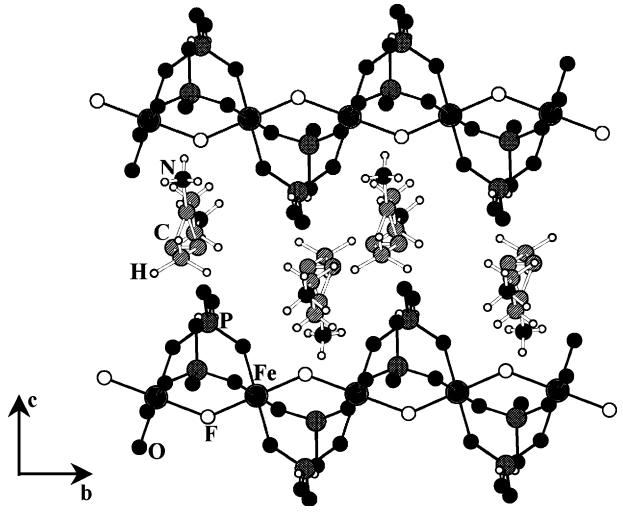

Fig. 4. Structure of **I** in the *bc* plane showing the tancoite chains and the amine molecules.

presence of different organic amine molecules have been reported earlier [2,4,5].

Mid strong hydrogen bonds between some oxygen atoms of the anionic inorganic chains and some hydrogen atoms of the diprotonated amines are also observed. The important hydrogen bond interactions are listed in Table 4.

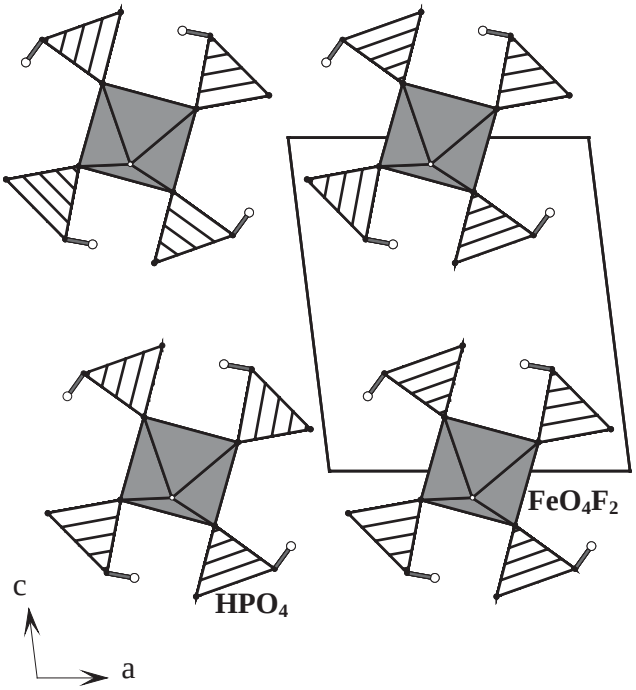

Fig. 5. Polyhedral connectivity of **I** in the *ac* plane showing the view down the chain axis.

Table 4
Important hydrogen bond distances in **I**, $[NH_3CH_2CH_2CH(NH_3)CH_2CH_3]^{2+}\,{}^{1}_{\infty}[FeF(HPO_4)_2]^{2-}$

D–H···A	D–H (Å)	H···A (Å)	D···A (Å)	D–H···A (°)
N(1)–H(1A)···O(6)	0.87	1.96	2.747(5)	150
N(1)–H(1B)···O(2)	0.91	2.10	2.972(2)	162
N(2)–H(2A)···O(4)	0.87	1.96	2.822(6)	166
N(2)–H(2B)···O(3)	0.80	2.09	2.883(5)	169
O(7)–H(30)···O(4)[a]	0.82	1.95	2.721(5)	156
O(5)–H(20)···O(6)[a]	0.82	1.90	2.714(5)	173

[a] Intra-chain.

Magnetic susceptibility studies on powdered single crystals have been performed on **I**. The temperature dependence of the inverse of magnetic susceptibility shown in Fig. 6 indicates a possible ordering at low temperatures. The fit of the high temperature magnetic susceptibility data and the resulting Curie–Weiss temperature ($\Theta_p \sim -160\,K$) is consistent with the presence of antiferromagnetic interactions. The magnetic moment obtained from the experimental data ($\sim 5\,\mu_B$), also indicates an oxidation state +3 for Fe. The anti-ferromagnetic interactions are through the F^- bridges that connect the Fe octahedra within the tancoite chain. The values of the Fe–F–Fe angle of $\sim 131^\circ$ is in agreement with this model [37]. Similar magnetic behavior has also been observed for

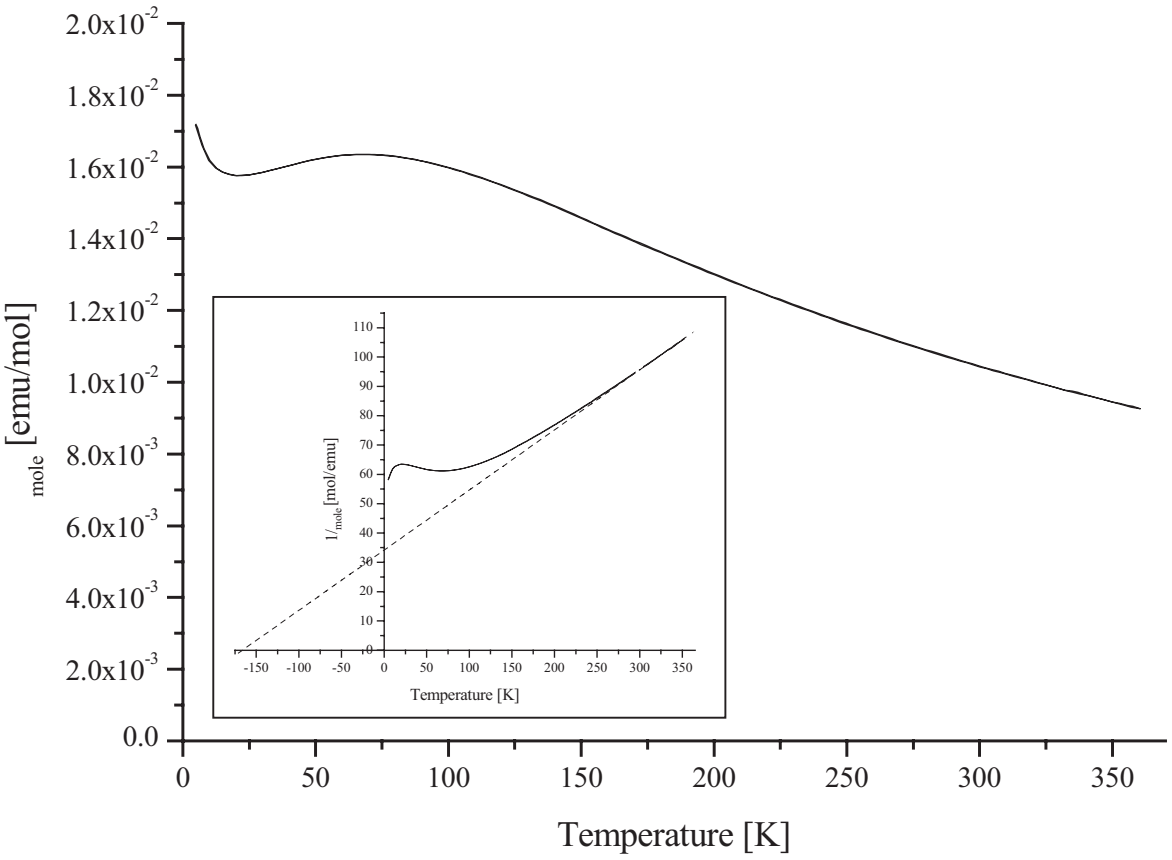

Fig. 6. χ vs. T plot for **I**, $[NH_3CH_2CH_2CH(NH_3)CH_2CH_3]^{2+}\ {}^{1}_{\infty}[FeF(HPO_4)_2]^{2-}$. Inset shows the $1/\chi$ vs. T plot.

other one-dimensional iron phosphates with tancoite related structure [2].

Acknowledgments

SN thanks the Department of Science and Technology (DST), Government of India, for the award of a research grant and SM the University Grants Commission (UGC), Government of India for the award of a research fellowship. SN also thanks the Royal Society of Chemistry for travel support under the *Travel Grant for International Authors* program and the Max-Planck-Gesellschaft for financial support.

References

[1] P.B. Moore, Am. Miner. 55 (1970) 135.
[2] M. Cavellec, D. Riou, J.-M. Greneche, G. Ferey, Inorg. Chem. 36 (1997) 2187.
[3] V. Zima, K.-H. Lii, J. Chem. Soc. Dalton Trans. 4109 (1998).
[4] Z.A.D. Lethbridge, P. Lightfoot, R.E. Morris, D.S. Wragg, P.A. Wright, Å. Kvick, G. Vaughan, J. Solid State Chem. 142 (1999) 455.
[5] S. Mahesh, M.A. Green, S. Natarajan, J. Solid State Chem. 165 (2002) 334.
[6] S. Mandal, S. Natarajan, J.M. Greneche, M.R. Cavellec, G. Ferey, Chem. Mater. 14 (2002) 3751.
[7] M. Cavellec, D. Riou, G. Ferey, J. Solid State Chem. 112 (1994) 441.
[8] M. Cavellec, D. Riou, G. Ferey, Eur. J. Solid State Inorg. Chem. 32 (1995) 271.
[9] M. Cavellec, D. Riou, G. Ferey, Acta Crystallogr. C51 (1995) 2242.
[10] M.R. Cavellec, J.M. Greneche, D. Riou, G. Ferey, Chem. Mater. 10 (1998) 1914.
[11] J.R.D. DeBord, W.M. Reiff, R.C. Haushalter, J. Zubieta, J. Solid State Chem. 125 (1996) 186.
[12] K.-H. Lii, Y.-F. Huang, Chem. Commun. 1311 (1997).
[13] V. Zima, K.-H. Lii, N. Nguyen, A. Ducouret, Chem. Mater. 10 (1998) 1914.
[14] A. Mgaidi, H. Boughzala, A. Driss, R. Clerac, C. Coulon, J. Solid State Chem. 144 (1999) 163.
[15] A.R. Cowley, A.M. Chippindale, J. Chem. Soc. Dalton Trans. 3425 (2000).
[16] A. Choudhury, S. Natarajan, C.N.R. Rao, Chem. Commun. 1305 (1999).
[17] A. Choudhury, S. Natarajan, Int. J. Inorg. Chem. 2 (2000) 217.
[18] A. Choudhury, S. Natarajan, J. Solid State Chem. 154 (2000) 507.
[19] M. Cavellec, D. Riou, G. Ferey, Inorg. Chim. Acta 291 (1999) 317.
[20] M. Cavellec, D. Riou, J.-M. Greneche, G. Ferey, J. Magn. Magn. Mater. 163 (1996) 173.

[21] M. Cavellec, D. Riou, C. Ninclaus, J.-M. Greneche, G. Ferey, Zeolites 17 (1996) 250.
[22] M. Cavellec, C. Egger, J. Linares, M. Nogues, F. Varret, G. Ferey, J. Solid State Chem. 134 (1997) 349.
[23] M. Cavellec, J.-M. Greneche, D. Riou, G. Ferey, Microporous Mater. 8 (1997) 103.
[24] M. Cavellec, J.-M. Greneche, G. Ferey, Microporous Mesoporous Mater. 20 (1998) 45.
[25] K.-H. Lii, Y.-F. Huang, Chem. Commun. 839 (1997).
[26] K.-H. Lii, Y-F. Huang, J. Chem. Soc. Dalton Trans. 2221 (1997).
[27] C.-Y. Huanh, S.-L. Wang, K.-H. Lii, J. Porous Mater. 5 (1998) 147.
[28] V. Zima, K.-H. Lii, J. Solid State Chem. 139 (1998) 326.
[29] J.R.D. DeBord, W.M. Reiff, C.J. Warren, R.C. Haushalter, J. Zubieta, Chem. Mater. 9 (1997) 1994.
[30] F.C. Hawthrone, Acta Crystallogr. Sec. B 50 (1994) 481 and the references therein.
[31] X-SHAPE version 2.01, STOE & CIE, Darmstadt, 2001.
[32] G.M. Sheldrick, SHELXTL-PLUS, ver. 6.12 Bruker AXS Inc., Madison, Wisconsin, USA, 2001.
[33] I.D. Brown, D. Altermatt, Acta Crystallogr. Sec. B 41 (1985) 244.
[34] G. Ferey, J. Fluorine Chem. 72 (1995) 187.
[35] G. Ferey, Chem. Mater. 13 (2001) 3084.
[36] R.A. Ramik, B.D. Sturman, P.J. Dunn, A.S. Poverennukh, Can. Mineral. 18 (1980) 185.
[37] J.B. Goodenough, Magnetism and the Chemical Bond, Interscience, New York, 1963.